Ind. J. Pharm. Edu. Res., 2026; 60(3):1159-1168.
https://www.ijper.org

Original Article

Synthesis, Structural Properties and Antibacterial Activity of Vorinostat Loaded on Carbon Nanotubes or Iron Oxide Nanoparticles

Dhulfiqar Abed[1,*], Saba Abdulmunem Habeeb[2], Lena Fadhil Al-Jibouri[3], Asmaa Hashim Hammadi[4], Noor Zuhair Kbah[5]

[1]Department of Pharmaceutical Chemistry, College of Pharmacy, Al Mustaqbal University, Babylon, IRAQ.
[2]Department of Pharmaceutical Chemistry, College of Pharmacy, University of Babylon, Babylon, IRAQ.
[3]Department of Clinical Laboratory Sciences, College of Pharmacy, University of Babylon, Babylon, IRAQ.
[4]Department of Pharmaceutics, College of Pharmacy, University of Babylon, Babylon, IRAQ.
[5]Department of Pharmaceutics, College of Pharmacy, Al-Zahraa University for Women, Karbala, IRAQ.

ABSTRACT

Background: In this work, Carbon Nanotubes (CNTs) and Iron Oxide Nanoparticles (IONPs) were successfully synthesized and their antibacterial activity were evaluated against *Staphylococcus aureus* (Gram-positive) and *Pseudomonus aeruginosa* (Gram-negative). Vorinostat, (SAHA) is a histone deacetylase inhibitor has recently shown the potential as an antibacterial agent through the genewration of Reactive Oxygen Species (ROS). **Materials and Methods:** Vorinostat (SAHA) was synthesized using conventional chemical reaction and characterized using FTIR, 1H-NMR and 13C-NMR. CNTs were synthesized using flame fragments deposition, and the IONPs were synthesized via co-precipitation method. SAHA was loaded on synthesized IONPs or CNTs, and the nanomaterial were analyzed using SEM, XRD, and FTIR. The antimicrobial activity of SAHA loaded IONPs or CNTs against gram positive and gram negative bacteria was quantitatively evaluated using agar well diffusion method. **Results:** SAHA was successfully characterized susing FTIR, 1H-NMR and 13C-NMR. Data from XRD analysis reveal appropriate loading of SAHA into the nanoparticles. The XRD analysis for the crystallite sizes of SAHA/ Fe_2O_3 and Fe_2O_3 nanoparticles were 54.2 and 38.4 nm, respectively. FTIR data indicated SAHA surface-bounding over the IONPs and CNTs in addition to SAHA encapsulation. No activity was observed against *Pseudomonas aeruginosa*, and a concentration dependent increase in the activity against *Staphylococcus aureus*. SAHA demonstrated a modest 120 mm inhibition zone against *S. aureus*. The inhibition zone increase considerably to 30-mm when 20 mg/mL of IONPs were used. Likewise, a 28 mm inhibition zone was produced with SAHA loaded CNTs. **Conclusion:** These results show that SAHA loaded nanostructures significantly increase their antibacterial activity against gram positive bacteria as a result of better drug delivery, membrane penetration, and increased oxidative stress. These results revealed the potential agonistic antibacterial activity of SAHA-loaded nanostructures, which could be associated with better drug delivery, membrane permeability, and increased oxidative stress in bacterial cell.

Keywords: SAHA, Carbon Nanotube (CNTs), Iron Oxide Nanoparticles, Antibacterial Activity, Drug Delivery.

Correspondence:
Dr. Dhulfiqar Abed
Department of Pharmaceutical Chemistry, College of Pharmacy, Al Mustaqbal University, Babylon-51001, IRAQ.
Email: abathur12@yahoo.com

Received: 25-12-2025;
Revised: 06-02-2026;
Accepted: 16-04-2026.

INTRODUCTION

The increasing bacterial resistance to traditional antibiotics is a great global health challenge today. In certain cases, bacterial strains produce slime, whereby they adhere and configure themselves into biofilms on artificial surfaces or implanted devices. This biofilm-building creates additional resistance in bacteria by stopping antibiotics from working effectively.[1,2] Various non-specific interactions, that is, electrostatic, dipole-dipole, hydrogen bonding, hydrophobic interactions, and vander waals forces, help bacteria to adhere to material surfaces, causing biofilm development.[2,3] Therefore, the material should ideally have certain antimicrobial properties that can potentially decrease micro-organism adhesion. To overcome this threat, there are many research groups worldwide developing pharmaceutical-grade Nanoparticles (NPs) as an alternate method of controlling microbial adhesion.[2] Nanoparticles in biological culture media interact with biological interfaces of cellular components like DNA, proteins, lipids, flavonoids, and polysaccharides. Their

DOI: 10.5530/ijper.20261673

behavior is affected by different physicochemical properties and the interactions at the nano-bio interface.[4] The biological interaction of nanoparticles with biologically relevant media involves their interactions with the other available functional groups and biomolecules such as lipopolysaccharides, phospholipids, and proteins on both the bacterial cell and eukaryotic membranes. These groups also promote the adhesion of bacteria to several surfaces and attach to new environments, giving rise to their establishment. Subsequently, the prospects for both the bacteria and the nanoparticles whether the bacteria will benefit from or be harmed by the nanoparticles will depend on the available groups on both bacterial surfaces and nanoparticle surfaces in conjunction with the physicochemical properties of the nanoparticles themselves.[4,5]

Regarding nanomaterial, the metal and metal oxide antibacterial properties have been evaluated, while some of these nanoparticles potentially create some health and environmental hazards.[5] Most of the transition metal ions such as those of iron, cobalt, and nickel and their compounds fall under metal nanoparticles. Iron Oxide Nanoparticles (IONPs) are being investigated because of their antimicrobial activity and lack of toxicity.[4]

The unique properties of CNTs make them as the most promising nanomaterials with biomedical, including large ratio of surface area to volume, and penetration ability to the cell membrane.[6] Carbon-based nanomaterials have attracted more and more attention of the researchers and scientists in many areas for the last few decades because of their outstanding physicochemical properties. Among the carbon nanostructures identified to find their applications are Carbon Nanotubes (CNTs), nano-diamond, fullerenes, and -fibers etc., of those, CNTs are the most widely used for biomedical applications. Once rolled up, graphene sheets form the hollow, concentric cylindrical structures known as CNTs that show an exceptional aspect ratio. To study CNTs antimicrobial activity, the interaction behavior between the CNTs and the microorganism have been reported.[7]

The ability of CNTs to penetrate cell wall which is related to its nanoscale size and high aspect ratio lead to the severe disintegration of the bacterial membrane and thereby bacterial death.[8,9]

The antibacterial action of IONPs may be due to the interaction with the bacterial cell membranes which results in disruption of membrane structure and eventually lead to apoptosis.[10] One of the CNTs mechanism as antibacterial, CNTs promote cell membrane phospholipid breakdown.[11] CNTs and IONPs could generate Reactive Oxygen Species (ROS) that damage components of living cells including lipids, proteins, and DNA, and thus lead to death in most bacteria. Therefore, beneficially remarkable properties of iron oxide nanoparticles and carbon nanotubes render them worthwhile for the idea of new antibacterial agents, given that the era we live in is challenged by increasing antibiotic resistance. The ability to disrupt bacterial membranes and to generate reactive species places them into a most promising position within the battle with bacterial infections and antibiotic resistance (Figure 1).[8,10]

Vorinostat, (SAHA, 1), is a histone deacetylase inhibitor in cancer therapy. Recently, research has investigated the possible antibacterial action of SAHA, notably in improving the efficacy of conventional antibiotics such as ciprofloxacin.[12] Vorinostat's antibacterial activity resulted from its ability to generate ROS. Vorinostat (SAHA) was selected in this study over other HDAe Ci because it recently identified dual function as anticancer and antibacterial agent particularly due to its capacity to produce ROS which contribute to the distruption of bacterial membrane and increase antibiotic effectiveness.

This effect can improve antibiotic efficacy, especially antibiotics that rely on oxidative processes for their antibacterial activity. For example, when bacterial cells are pretreated with vorinostat, studies have shown a remarkable increase in the zones of inhibition and a decrease in the Minimum Inhibitory Concentration (MIC) values for ciprofloxacin across different bacterial strains.[12] Figure 1 illustrates the proposed mechanism of antibacterial activity of SAHA, IONPs, and CNTs. This study focused on developing a drug loaded nanocomposite model with antimicrobial properties for treatment of bacterial infections. The goal was to explore the antibacterial effect of our drug loaded nanocomposite model. The study investigated vorinostat (SAHA) loaded onto CNT or iron oxide nanoparticles as a potential antibacterial treatment against *Staphylococcus aureus* (gram-positive) and tested its antibacterial effect on *Pseudomonas aeruginosa* (gram-negative).

MATERIALS AND METHODS

Liquefied petroleum gas is from Iraq-Babylon Governorate market. The ingredients utilized in this experiment were 30% H_2O_2 (hydrogen peroxide) from Barcelona, Scharlab Spain. The standard MWNTs in this work had a mode 5.5 nm in diameter and a purity of 95%, which was used in comparison with produced CNTs. None of the materials needed to be further purified before usage. All chemical synthesis reagents were of ACS grade and did not need any further purification. ACS reagent grade solvents

Table 1: Antibacterial evaluation of IONPs, SAHA, and SAHA loaded IONPs.

sample	Zone of inhibition in diameter (in mm)	
	S. aureus	*P. aeruginosa*
Fe1	0	0
Fe2	5	0
Fe3	12	0
Drug	12	0
Fe1+D	12	0
Fe2+D	25	0
Fe3+D	30	0

were bought. For reaction monitoring, we used silica gel plates, aluminum-backed was used, and these were visualised using UV light. The spectra of 1H NMR and 13C NMR were recorded using the Bruker Multinuclear NMR spectrometer with $DMSOd_6$ as a solvent. Regarding the NMR data, the resonance frequencies that were expressed in parts per million (ppm) units.

Methods

Synthesis of Iron Nanoparticles

At room temperature, a 10 g of $FeCl_3.6H_2O$ was dissolved in clean water (150 mL) with stirring. Then, slowly add 10 drops of dilute ammonia solution to the swirling mixture at room temperature and at a rate of 1 mL/min. While maintaining pH of 1 during nanoparticles preparation, the black dispersion was swirled constantly at room temperature for 60 min and then for 120 min at 80°C. Then, upon completion, a brown solid was formed when the reaction mixture cooled down to room temperature. The brown solid product calcined for 4 hr at 500°C and then analyzed without washing or further purification.[13]

Synthesis of Carbon Nanotubes

This section describes the synthesis of Carbon Nanotubes (CNTs) utilizing the flame fragments deposition method using a homemade chamber instrument produced from natural gas from Iraq as the carbon source. The instrument is made up of nine collection centers that are inserted in each position at the top.[14]

Synthesis of N-hydroxy-N′-phenyl-octanediamide, (Vorinostat, SAHA, 1)

To Octanedioic acid (1.742 g, l.0 eq) in tetrahydrofuran (15 vol) solution chilled to 0- 5°C, triethylamine (1.52 mL, 1.1 eq) and Methyl chloroformate (0.77 mL, l.l eq) were added and stirred for 15 min. Then, filter the HCl salt and add (0.91 mL, leq) aniline to the mixture by stirring for 15 min at 0-5°C. After that, (1.52 mL, l.leq) of triethylamine and (0.77 mL, l.leq) of Methyl chloroformate were added to the mixture with stirring at 0-5°C for 15 min. Then add methanolic solution of hydroxylamine (preparation below) cooled at 0-5°C which was prepared instantly with continuous stirring for 15 min. Upon completion, the organic solvent was removed, and the residue was taken in dichloromethane. The organic layer was washed with water and dried over magnesium sulfate. The organic layer was removed, and the residue was taken into acetonitrile. Then, stir the mixture for 15 min, and filter to afford the desired product as a white solid (810 mg, 31%) (Scheme 1).[15]

Preparation hydroxylamine solution:

To the solution Potassium hydroxide (0.62 g, l.leq) in methanol (8vol) at 0-5°C, hydroxylamine hydrochloride (0.76 g, l.leq) in methanol (8vol) solution at 0-5°C was added and stirred at same temperature. Then, the salt was filtered off and the filtrate was taken for the reaction. 1H NMR (400 MHz) (DMSO-d6) δ) 9.85 (1H, s, amide -NH-), 8.78 (1H, s, -OH), 7.59 (2H, t, J=7.65 Hz), 7.28 (2H, t, J=7.90 Hz), 7.01 (1H, t, J = 7.35 Hz), 2.29 (2H, t, J=7.4 Hz, methylene), 1.95 (2H, t, J=7.3 Hz, methylene), 1.58 (2H, m, methylene), 1.50 (2H, m, methylene), 1.32-1.25 (2H, m, methylene). 13C NMR (100 MHz) (DMSO-d6) δ 171.71, 169.62, 139.81, 129.08, 123.38, 119.52, 36.85, 32.72, 28.89, 28.87, 25.51.

Purification Processes

The produced CNTs were purified by two different methods. The first involved treatment with H_2O_2 only, while the second involved treatment with H_2O_2 then by acetone using a separating funnel. For 60 min., 100 mg of the produced CNTs were dispersed in H_2O_2 (50 mL) using an ultrasonic water bath. The mixture kept at 4°C for 24 hr followed by heating at 50°C until complete removal of H_2O_2. The sample was then dried for 4 hr at 80°C after being cleaned with deionized water. The second method used acetone in the same methods for the dry sample. CNTs are dissolved in 15 mL of acetone as part of the acetone treatment. For 15 min, there was a sonication suspension. After that, centrifuge the suspension for fifteen min. After that, the separated CNTs were calcined for 2 hr at 275°C.[16]

The generated CNTs after sequential treatment with H_2O_2 followed by acetone showed descending evidence of having CNTs structure with a length of 0.8-2.1 μm with a tubular structure.[16] CNT sizes range from 26.91 to 31.62 nm.[14]

Functionalization of Carbon Nanotubes

An essential step that can be used to improve the surface properties of carbon nanotubes is functionalization, which adds certain functional groups to the surface. In round bottom flask, 100 mg of CNTs were dispersed in 75 mL of 30% H_2O_2 and the reaction mixture flask related to a condenser. Then, the mixture is refluxed overnight at 80°C. Following reflux, the suspension of carbon nanotubes and H_2O_2 was dried by heating it to 50°C and exposing it to UV light for 5 hr. To create the composite, the surface oxidation of carbon nanotubes is crucial. The establishment of hydrogen bonds in distilled water causes the homogenous spread of O-CNTs. Utilizing FTIR, the produced functional O-CNTs were studied.[17]

Table 2: Antibacterial evaluation of IONPs, SAHA, and SAHA loaded IONPs.

Sample	Zone of inhibition in diameter (in mm)	
	S. aureus	*P. aeruginosa*
CNT1	0	0
CNT2	0	0
CNT3	10	0
Drug	12	0
CNT1+D	15	0
CNT2+D	15	0
CNT3+D	28	0

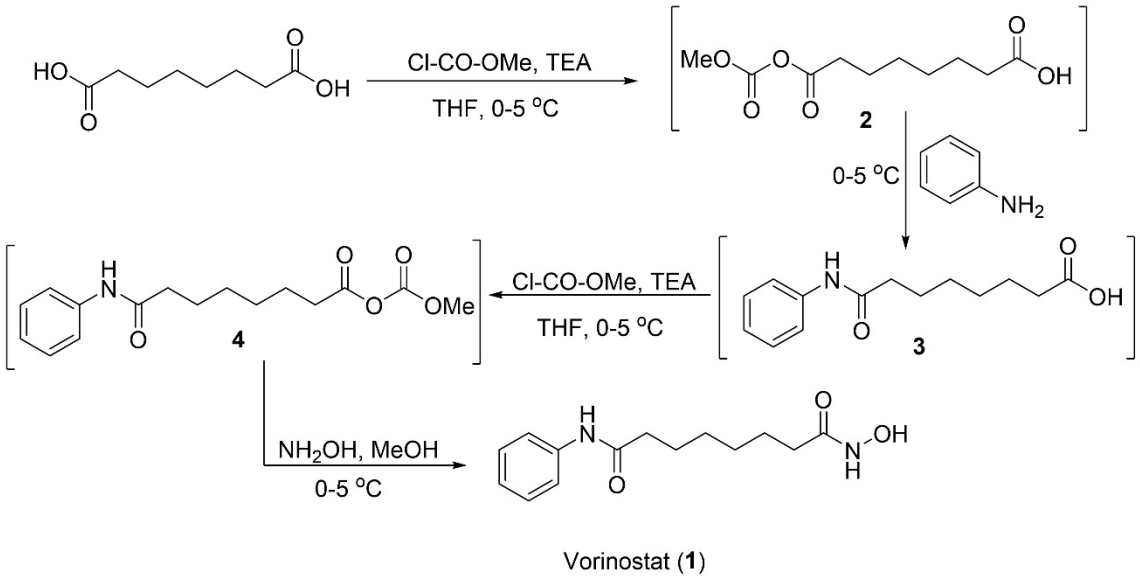

Scheme 1: Synthesis of Vorinostat(1).

Synthesis of Vorinostat (SAHA, 1)

As outlined in Scheme 1, Vorinostat (1) was synthesized using commercially available Suberic acid. Treatment of acid with Methyl chloroformate in the presence of base in tetrahydrofuran (anhydrous) at 0-5°C to give anhydride intermediate 2. Then amide intermediate 3 was synthesized by adding aniline to the reaction mixture while maintaining the reaction mixture at 0-5°C followed by addition of Methylchloroformate in the presence of as a base in tetrahydrofuran (anhydrous) at 0-5°C to get anhydride intermediate 4. Treatment of anhydride intermediate 4 with hydroxylamine solution in methanol at 0-5°C gave final compound Vorinostat (SAHA, 1).[15]

Loading SAHA on Nanostructure

Suberoylanilide hydroxamic acid loading on O-CNT was carried out by first making an aqueous solution of SAHA (40 mg/10 mL) and then distributing three different concentrations of CNTs (CNT1, CNT2 or CNT3) or Fe_2O_3 nanoparticles (Fe1, Fe2, Fe3) at (5, 10, and 20 mg/mL) into the SAHA solution. To get rid of the dissociative SAHA, the mixture was shaken for 48 hr in the dark, then slowly centrifuged at room speed (10.000 rpm) and cleaned with PBS (phosphate-buffered saline) solution (pH=6.8). After obtaining SAHA/CNTs or SAHA/Fe_2O_3, they were dried under vacuum at room temperature and sealed for further use.[18]

Antibacterial Activity

The agar well diffusion method evaluated the antibacterial activity of SAHA (40 mg/mL) loaded on synthesized CNTs and Fe_2O_3 nanoparticles (5, 10, 20) mg/mL. The activity was tested against *S. aureus* and *P. aeruginosa*. At room temperature, the PH of Mueller-Hinton agar medium should be 7.2 to 7.4. Initially, agar plates were used to select well-isolated colonies. Next, a wire loop was used to move each bacterial colony to a test tube with 4 to 5 mL of nutritional broth medium. Then incubate broth culture at 35°C till the culture met or surpassed the McFarland criteria for turbidity of 0.5. A sterile swab with an applicator was dipped into the modified suspension within 15 min of the inoculum suspension's turbidity being altered. To get rid of extra inoculum, the swab was turned several times and firmly pressed against the tube's interior wall above the fluid level. The Mueller-Hinton agar plates were dried, and the entire sterile agar surface was streaked with a swab to inoculate it. After that, the plates were put back on top, and for three to 5 min, materials for the nanoparticles were applied while any extra surface moisture was absorbed. Using sterile forceps, a suitable well (no closer than 35 mm from center to center) was created on the agar plate's surface to maximize the nanomaterial's diffusion. On a 150 mm plate, no more than six wells should be cut. The nanomaterial suspension that had been previously prepared was added to the wells. Once the wells were correctly cut, the plates were in an incubator set at 37°C for 15 min under aerobic conditions. After incubation for 16-18 hr, thorough plate inspection was performed. The zone inhibition was measured manually using a rule to measure the zones of inhibition diameters, which included the well's diameter. Following analysis, the zone sizes correspond to the organism were reported.[19]

Characterization

Scanning electron microscope photos were used to establish morphology. SEM (XL30 FEG; Philips) was used to evaluate the morphology of the resulting formulations. To find the standard deviation, average diameter, and particle size distribution for each formulation, 300 particles were sized using Image J software. Using transmission electron microscopy (Carl Zeiss EM900, Germany), JEM 2100 examined the interior morphology of the material. We measured the MCM-41 position, crystalline structure, and structural characteristics of in the range of 0°-100° and at rate of

10 (deg/min) using the X-ray diffract pattern. Cu K (=1 0.541°A) was the source of the X-ray radiation (XRD: PW1730: Philips). With the (FT-IR) infrared spectra in transmission mode, a (SHIMADZU FT-IR 8400S).

RESULTS AND DISCUSSION

Scanning Electron Microscopy SEM

The dispersion of CNTs might be shown by using the Scanning Electron Microscopy (SEM) technique because of its crisp images, high resolution, and three-dimensional representation. SEM analysis produced similar outcomes. The pictures of the synthetic CNTs are displayed in Figure (2a). Figure 2 displays the SEM micrographs of the loaded samples with CNTs, SAHA, and SAHA/CNTs. Figure (2a) of CNTs displays a flat surface with entangled and curled tubes, whereas Figure (2b) of SAHA shows crystals. In contrast, the surfaces of the CNTs in the PM sample (Figure 2c) were rough and had some connected clusters, suggesting that the carbon nanotubes were simply combined. When physically combined with CNTs, SAHA stuck to their surface rather than forming a complex. In contrast, the SAHA crystal vanished for the SAHA/CNTs, revealing irregularly sized blocks-like structural characteristics (Figure 2c). The host- guest relationship between SAHA and CNTs may be the cause of the notable morphological alteration. SAHA-loaded CNTs had a greater average diameter (36 nm) compared to CNTs (29 nm). The synthetic iron oxide sample's morphology was verified by SEM examination (Figure 3a). The spherical shape of the Fe_2O_3 nanoparticles is evident from the results obtained from scanning electron microscopy investigation. Supplementary Figure (3c) displays the SEM image of Fe_2O_3 nanoparticles loaded with SAHA. Since the nanoparticles had a smooth, spherical form, the slower drug release could have resulted from their smooth surface.

X-ray Powder Diffractometry (XRD)

XRD is a helpful method to determine the crystalline formation. Figure 4 displays the Fe_2O_3, SAHA, and SAHA/Fe_2O_3 samples' X-ray diffractograms. Fe_2O_3 is present in the sample, as shown by the XRD pattern shown in Figure 4a, where the peaks (012), (104), (110), (113), (024), (118), (123), (213), and (300) appear. According to the narrow form peaks of the materials (diffraction peaks), we can confirm the good crystallinity without impurities phase of hematite (Fe_2O_3) and goethite α-FeO (OH). These peaks are (104) and (110) at 2θ positions, 21.22° and 33.15°.[20,21] SAHA diffractogram, a crystalline solid, showed distinct crystalline peaks (Figure 5B).[21] The sharpness and strength of the peaks in the vorinostat's diffraction pattern proved its crystalline structure. Vorinostat revealed six significant peaks at 10.54°, 16.63°, 19.75°, 21.09°, 23.55°, and 25.35°. The aforementioned peaks appear in the XRD pattern of the Vorinostat-loaded Fe_2O_3 implant, but with less intensity than that of the pure medication and Fe_2O_3.

However, examination of the SAHA/Fe_2O_3 combination revealed that the SAHA sample's diffractogram had distinct, crisp crystalline peaks (Figure 4c). Particle sizes were correlated with

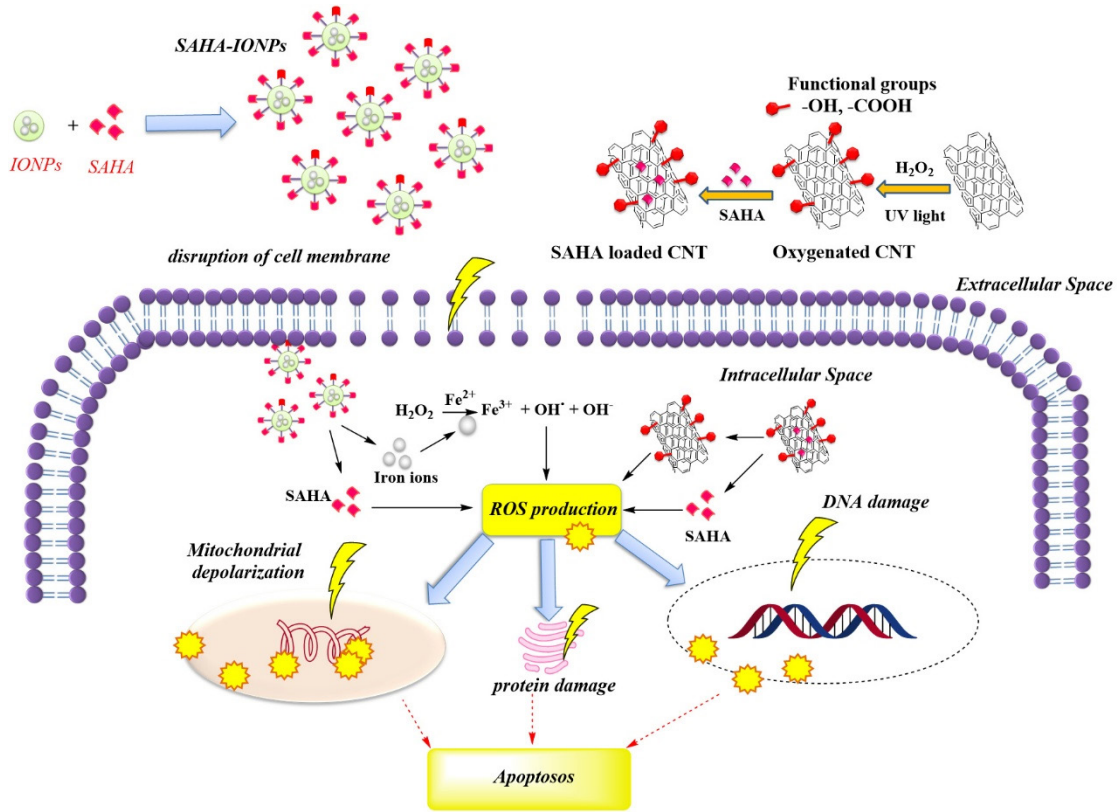

Figure 1: Schematic mechanisms for the proposed antibacterial effects of SAHA loaded on IONPs or CNTs.

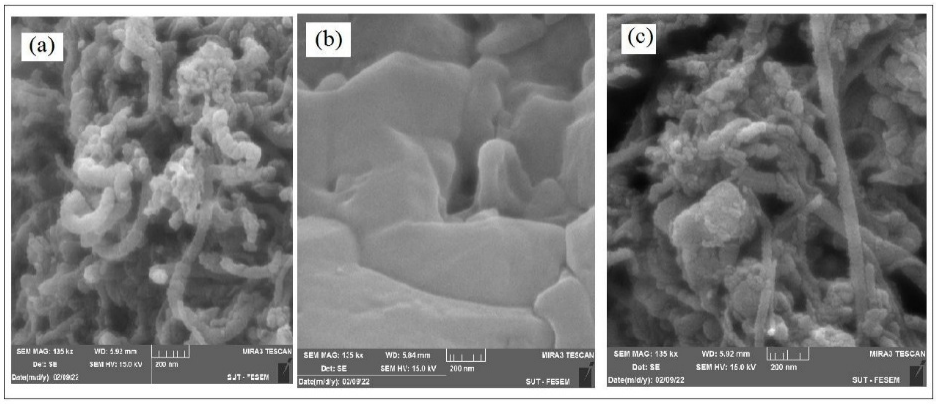

Figure 2: SEM for (a) CNTs, (b) SAHA, and (c) SAHA/ CNTs loaded.

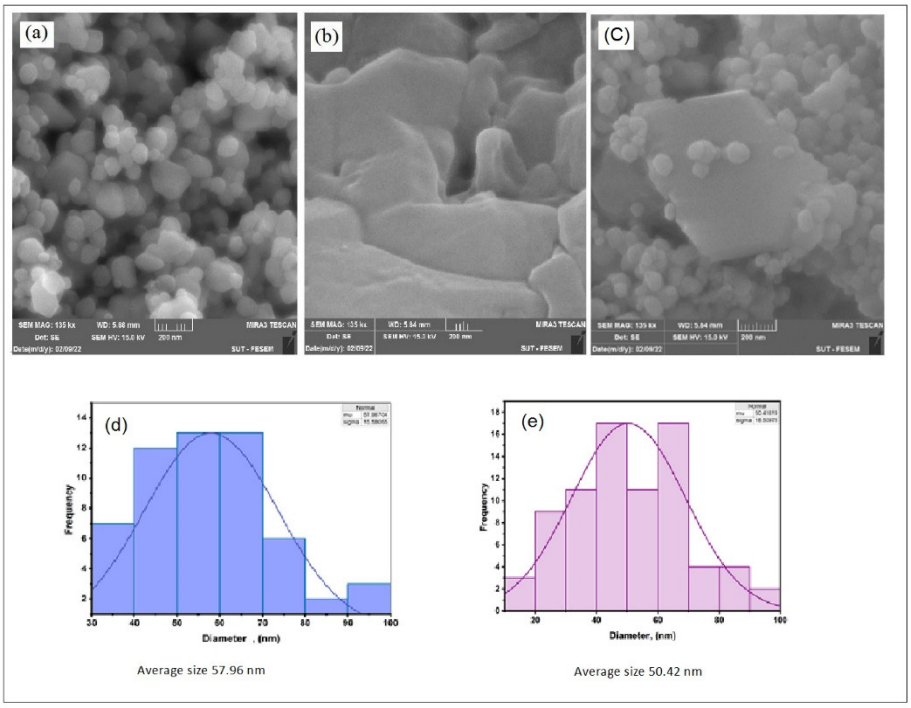

Figure 3: SEM for (a) Fe2O3,(b) SAHA, (c) SAHA/ Fe2O3 loaded,(c) Particle size distribution histogram of Fe2O3,(e) Particle size distribution histogram of SAHA / Fe2O3.

the diffraction peaks' broadness. The average particle size D was determined using Scherrer's equation.[22] The SAHA/ Fe_2O_3 and Fe_2O_3 nanoparticles were estimated to have mean crystallite sizes of 54.2 and 38.4 nm, respectively.

The XRD pattern of CNTs, SAHA, and CNTs/SAHA surface is shown in Figure 5. Figure 3 displays the synthesized CNTs' XRD spectrum, which is taken from Figure 5a. There are numerous broad bands in the XRD diffraction patterns, including peaks at 26.0° and 43.2°. Because of the existence of carbon atoms, graphite exhibits a peak at 26.0° with inter-planar spacing. The nanotube structure is characterized by the peaks around 43.2°.[23,24] Vorinostat by alone exhibits distinct crystalline peaks in Figure 5b. These findings showed that vorinostat was molecularly dispersed throughout the nanoparticle matrix and that its intrinsic crystallinity was reduced upon integration into the CNTs. The sharpness and strength of the peaks in the vorinostat's diffraction pattern proved its crystalline structure. Vorinostat revealed six major peaks at 10.54°, 16.63°, 19.75°, 21.09°, 23.55°, 25.35°, 27.26°, and 29.21°. The aforementioned peaks appear in the XRD pattern of the vorinostat-loaded CNTs implant, albeit with more intensity than that of the pure drug, particularly the peak 27.26°.

Furthermore, as shown in (Figure 5c), these data reveal appropriate loading of SAHA into the nanoparticles.

Fourier Transform Infrared Spectroscopy (FTIR)

Initially, we evaluated the che1mical stability of our drug and nanomaterials using FTIR as illustrated in Figure 6. Figure 6a displays the strong characteristics of functionalized Carbon

Nanotubes (CNTs) as well as a wide band from 3173 to 3600 cm^{-1} corresponds to stretching vibrations of hydroxyl group.[25]

Regarding the carbonyl group stretching vibrations in aldehyde, carboxylic acid, and acid anhydride group, a broad band between 1766 and 2017 cm^{-1}.[26,27] Based on FTIR peaks for SAHA, and SAHA-loaded CNTs, we were able to identify the characteristic SAHA peaks at fingerprint region. These data indicated SAHA surface- bounding over the CNTs in addition to SAHA encapsulation. Peaks at 3500 cm^{-1} (O-H stretching, 2900 and 3100 cm^{-1} corresponding to stretching vibrations =C-H, 2950 and 3000 cm^{-1} (C-H stretching), 1758 cm^{-1} (C=O stretching), 1150 and 1300 cm^{-1} (C-C(=O)-O- stretching), 999-1012 cm^{-1}, and displayed a peak at 1007 cm^{-1} attributed to planar deformations. SAHA-loaded CNTs showed identical spectra to SAHA, except for a shift in the peak for O-H stretching vibrations from 3500 to 3288-3399 cm^{-1} (Figure 6).

We used FTIR to monitor any changes in the characteristic peak shape, frequency, and location to determine the creation of the IONPs, SAHA, and SAHA/ Fe_2O_3. Figure 7 shows that the FTIR spectrum for IONPs, SAHA, and SAHA/ IONPs which was used to identify the functional groups and chemical bonds.[28,29] The FTIR broad peak at 3398 cm^{-1} corresponds to the OH stretching vibration in OH groups. The IR peaks around 1604 cm^{-1} and 1487 cm^{-1} are attributed to the carbonyl bending vibration whereas the IR peak at 1293 cm^{-1} corresponds the poly(vinylpyrrolidone) group.

Fe-O stretching mode is given to the strong band below 700 cm^{-1}. At 576 cm^{-1}, the band associated with the Fe-O stretching mode of Fe_2O_3 is seen. The SAHA spectrum (Figure 7B) showed the distinctive peaks of SAHA and was in good agreement with other literature.[18,30] The SAHA's peak intensity is being reduced.

The infrared spectrum of SAHA/ Fe_2O_3 shows a band at 3446 cm^{-1} for the stretching of the -OH group, bands at 1760 cm^{-1} for the C=O group, bands at 1614, 1504, and 1459 cm^{-1} for C=C aromatic group stretching, and a band at 500 cm^{-1}.

Antibacterial Activity

Based on data from agar well diffusion method, it has been found concentration dependent effect of SAHA loaded IONPs or CNTs on *Staphylococcus aureus*, while *Pseudomonas aeruginosa* is not affected by these nanoparticles at different concentration. The best concentration of CNTs (20 mg/ mL) with drug (40 mg/mL) that exhibit the best antibacterial activity. Regarding SAHA loaded IONPs, 20 mg/ mL of IONPs with drug concentration 40 mg/mL. Furthermore, a concentration dependent effects of SAHA loaded on IONPs/or CNT on gram-positive bacteria have been reported as shown in the following Tables 1 and 2.

Gram-positive bacteria are effect by the synthesized nanoparticles while Gram-negative bacteria is not affected. The difference in activity for our prepared nanomaterial may be attributed to the morphology differences between these bacteria. The outer

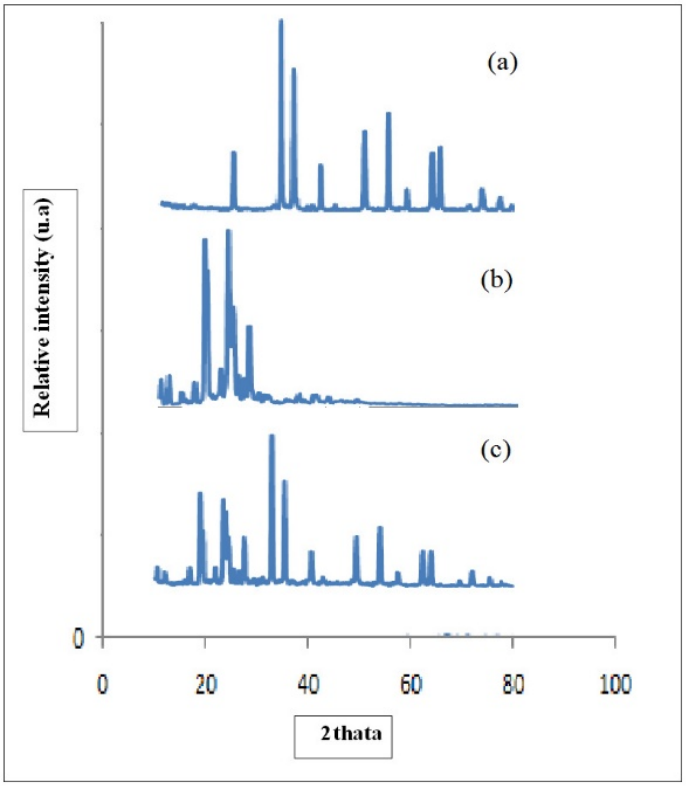

Figure 4: XRD for (a) Fe2O3,(b) SAHA, and (c) SAHA/ Fe2O3 loaded.

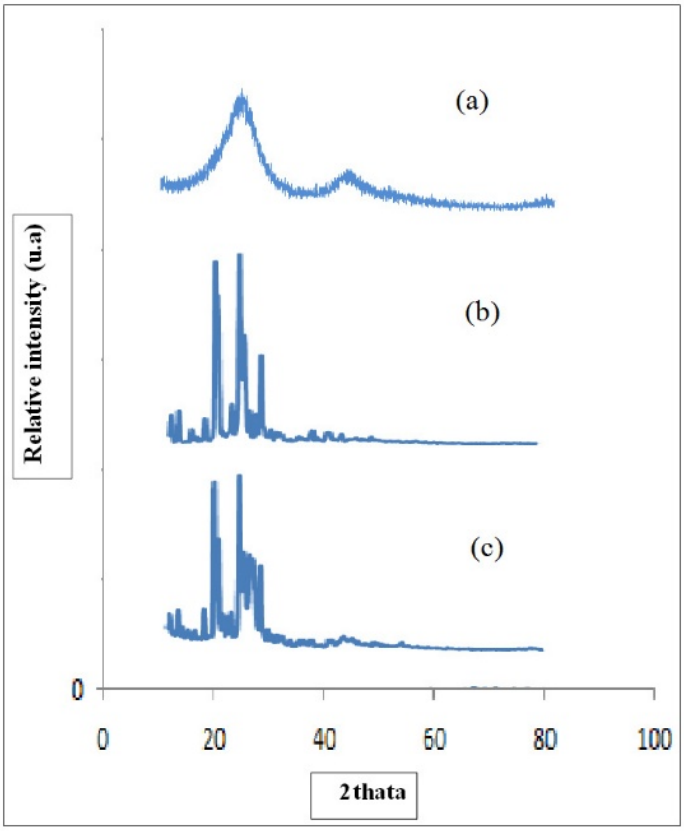

Figure 5: XRD for (a) CNTs,(b) SAHA, and (c) SAHA/ CNTs loaded.

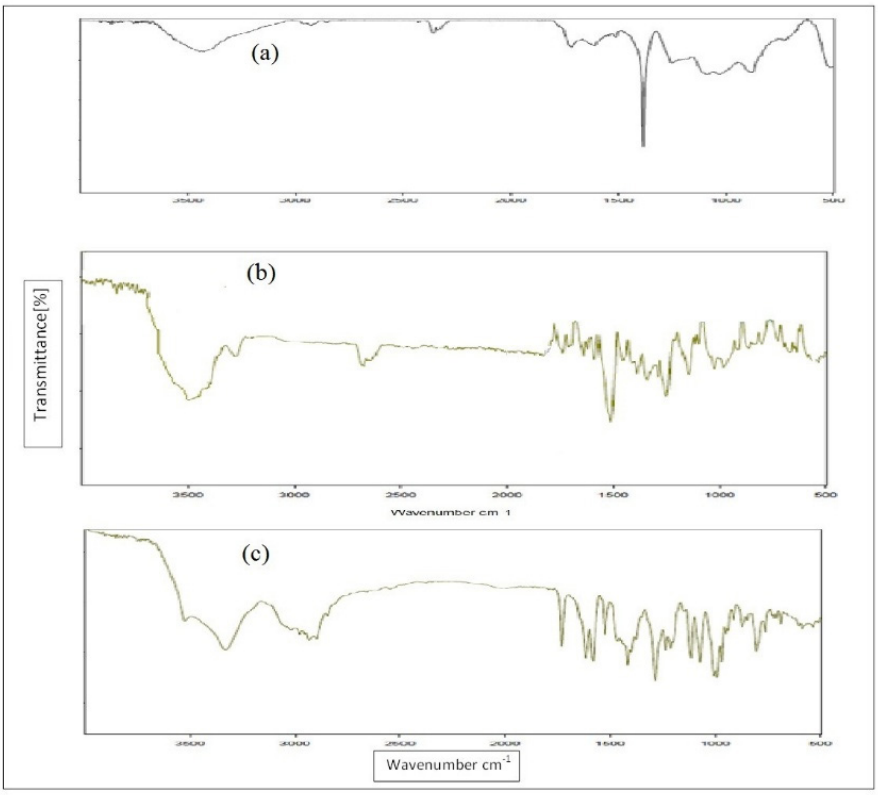

Figure 6: FTIR for (a) CNTs,(b) SAHA, and (c) SAHA/ CNTs loaded.

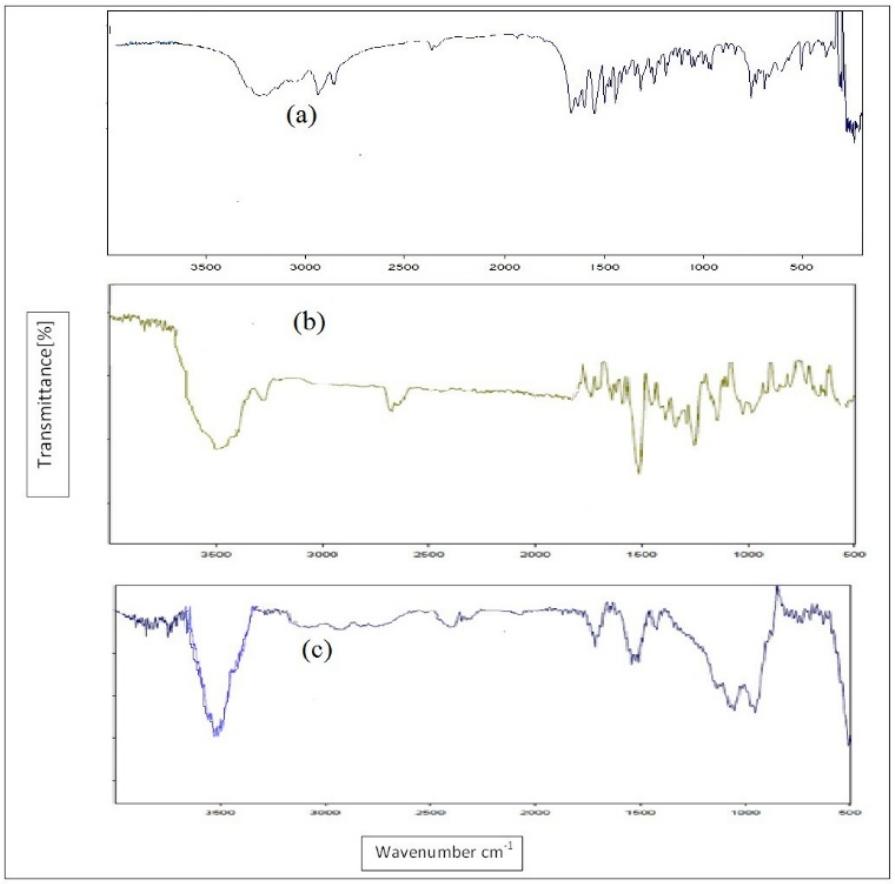

Figure 7: FTIR for (a) Fe2O3,(b) SAHA, and (c) SAHA/ Fe2O3 loaded.

polysaccharide membrane in Gram-negative bacteria makes it more resistant. On the other hand, the outer peptidoglycan layer in Gram-positive bacteria makes it more susceptible.[30]

CONCLUSION

In our study, CNTs, IONPs and SAHA loaded on these nano-systems were achieved successfully. Analysis of these nanomaterials were done using SEM, XRD, and FTIR. Data from XRD analysis reveals appropriate loading of SAHA into the nanoparticles. The XRD analysis for the crystallite sizes of SAHA/$Fe_2O_3$and Fe_2O_3 nanoparticles were 54.2 and 38.4 nm, respectively. The FTIR analysis confirmed SAHA surface- bounding over the CNTs in addition to SAHA encapsulation. The antibacterial activity against *Staphylococcus aureus* and *Pseudomonas aeruginosa* was measured. The concentration shows the most effective antibacterial action against gram-positive bacteria was the 20 mg/mL mixed with 40 mg/mL of SAHA drug and concentration of iron oxide nanoparticles 20 mg/mL mixed additionally with 40 mg/mL of drug. The antibacterial activity for the CNTs and IONPs was higher against gram-positive *Staphylococcus aureus* than for gram-negative bacteria *Pseudomonas aeruginosa*. This may be attributed to the differences in structural, biochemical, and genetic properties. The potential agonistic properties of SAHA-loaded nanomaterials (CNTs/IONPs) could be associated with enhancing oxidative stress in bacterial cells. These results may indicate the potential of these SAHA loaded nanomaterial as antimicrobial agents. In translating these promising findings into clinical applications present several challenges, including biocompatibility and safety studies of SAHA loaded nanomaterials. Comprehensive preclinical toxicological studies are essential to evaluate these challenges.

ACKNOWLEDGEMENT

The authors would like to sincerely thank the University of Babylon College of pharmacy and the university of Al Mustaqbal College of pharmacy for valuable support and contribution to this work.

ABBREVIATIONS

CNTs: Carbon Nanotubes; **Fe1, Fe2, Fe3:** Iron oxide nanoparticle concentrations (5, 10, and 20 mg/mL, respectively); **$FeCl_3 \cdot 6H_2O$:** Iron (III) chloride hexahydrate; **FTIR:** Fourier Transform Infrared Spectroscopy; **HDAe Ci:** Histone deacetylase inhibitor; **H_2O_2:** Hydrogen peroxide; **IONPs:** Iron oxide nanoparticles; **LT:** Luteolin; **MIC:** Minimum inhibitory concentration; **MWNTs:** Multi-walled nanotubes; **NMR:** Nuclear magnetic resonance; **NO:** Nitric oxide; **NPs:** Nanoparticles; **O-CNT:** Oxidized carbon nanotubes; **OVA:** Ovalbumin; **PBS:** Phosphate-buffered saline; **PM:** Physical mixture; ***P. aeruginosa:*** *Pseudomonas aeruginosa*; **RH:** Research Heading; **ROS:** Reactive oxygen species; ***S. aureus:*** *Staphylococcus aureus*; **SAHA:** Suberoylanilide hydroxamic acid (Vorinostat); **SEM:** Scanning electron microscopy; **TEM:** Transmission electron microscopy; **UV:** Ultraviolet; **XRD:** X-ray diffractometry; **δ:** Chemical shift; **µm:** Micrometers; **°C:** Degrees Celsius.

CONFLICT OF INTEREST

The authors declare that there is no conflict of interest.

SUMMARY

The rise of bacterial resistance and biofilm formation has created an urgent need for alternative antibacterial strategies. Nanoparticles (NPs), particularly Iron Oxide Nanoparticles (IONPs) and Carbon Nanotubes (CNTs), offer antimicrobial potential due to their physicochemical properties, ability to disrupt bacterial membranes, and capacity to generate Reactive Oxygen Species (ROS). CNTs possess high surface area and membrane-penetrating ability, while IONPs interact with bacterial membranes and induce apoptosis. Vorinostat (SAHA), a histone deacetylase inhibitor with emerging antibacterial activity, enhances oxidative stress and improves antibiotic efficacy through ROS production. In this study, SAHA was synthesized and successfully loaded onto functionalized CNTs and IONPs. Nanomaterials were characterized using SEM, XRD, and FTIR, confirming proper morphology, crystallinity, and drug loading. Antibacterial testing via agar well diffusion showed concentration-dependent activity of SAHA-loaded CNTs and IONPs against Staphylococcus aureus (gram-positive), while Pseudomonas aeruginosa (gram-negative) showed no sensitivity, likely due to its protective outer membrane. The most effective formulations were 20 mg/mL CNTs or IONPs loaded with 40 mg/mL SAHA. Findings indicate that SAHA-loaded nanocomposites have promising antibacterial potential, though further studies on biocompatibility and safety are necessary before clinical use.

REFERENCES

1. Lal AF, Gupta PS. An Exploration of Chrysin Fabricated Silver Nanoparticles as Antibiofilm Agent against Pseudomonas aeruginosa. Indian Journal of Pharmaceutical Education and Research. 2024; 58(2s):s429-s35.
2. Grooters KE, Ku JC, Richter DM, Krinock MJ, Minor A, Li P, *et al.* Strategies for combating antibiotic resistance in bacterial biofilms. Frontiers in cellular and infection microbiology. 2024;14:1352273.
3. Saravanan K, Bharathi M, Alyami NM, Alharbi SA, Hussein-Al-Ali SH, Arulselvan P. Synthesis and Characterization of Novel Chitosan-Nickel oxide Based Amygdalin Hybrid Nanomaterials for Antibacterial and Anticancer Properties. Indian Journal of Pharmaceutical Education and Research. 2024;58(4):1225-34.
4. Zhang T-G, Miao C-Y. Iron Oxide Nanoparticles as Promising Antibacterial Agents of New Generation. Nanomaterials. 2024;14(15):1311.
5. Vasić K, Knez Ž, Leitgeb M. Multifunctional Iron Oxide Nanoparticles as Promising Magnetic Biomaterials in Drug Delivery: A Review. Journal of functional biomaterials. 2024;15(8):227.
6. Anzar N, Hasan R, Tyagi M, Yadav N, Narang J. Carbon nanotube-A review on Synthesis, Properties and plethora of applications in the field of biomedical science. Sensors International. 2020;1:100003.
7. Hassani M, Tahghighi A, Rohani M, Hekmati M, Ahmadian M, Ahmadvand H. Robust antibacterial activity of functionalized carbon nanotube-levofloxacine conjugate based on *in vitro* and *in vivo* studies. Scientific Reports. 2022;12(1):10064.
8. Song B, Xu P, Zeng G, Gong J, Zhang P, Feng H, *et al.* Carbon nanotube-based environmental technologies: the adopted properties, primary mechanisms, and challenges. Reviews in Environmental Science and Bio/Technology. 2018;17:571-90.

9. Saleemi MA, Kong YL, Yong PVC, Wong EH. An overview of antimicrobial properties of carbon nanotubes-based nanocomposites. Advanced Pharmaceutical Bulletin. 2022;12(3):449.
10. Mammari N, Lamouroux E, Boudier A, Duval RE. Current knowledge on the oxidative-stress-mediated antimicrobial properties of metal-based nanoparticles. Microorganisms. 2022;10(2):437.
11. Marghade D, Karunanidhi D. Properties and adsorption mechanism of biological contaminants by carbon nanotubes. Water Treatment Using Engineered Carbon Nanotubes: Elsevier; 2024. p. 271-305.
12. Misztak P, Sowa-Kućma M, Szewczyk B, Nowak G. Vorinostat (Saha) may exert its antidepressant-like effects through the modulation of oxidative stress pathways. Neurotoxicity Research. 2021;39:170-81.
13. Farahmandjou M, Soflaee F. Synthesis and characterization of α-Fe2O3 nanoparticles by simple co-precipitation method. Physical Chemistry Research. 2015;3(3):191-6.
14. Hammadi AH, Abdulrazzak FH, Atiyah AJ, Hussein FH. Synthesis of Carbon Nano tubes by Flame Fragments Deposition of Liquefied Petroleum Gas. Org Med Chem Int J. 2017;29(12):2804-8.
15. Gaitonde A, Choudhari B. Novel process for the preparation of vorinostat. Google Patents; 2009.
16. Hammadi AH, Jasim AM, Abdulrazzak FH, Al-Sammarraie AM, Cherifi Y, Boukherroub R, *et al.* Purification for carbon nanotubes synthesized by flame fragments deposition via hydrogen peroxide and acetone. Materials. 2020;13(10):2342.
17. Hammadi AH, Assi LN, Hussien FH, Hussien FH. Drug Loading on Carbon Nanotubes synthesized by Flame Fragments Deposition Technique. Systematic Reviews in Pharmacy. 2020;11(3).
18. Sankar R, Karthik S, Subramanian N, Krishnaswami V, Sonnemann J, Ravikumar V. Nanostructured delivery system for Suberoylanilide hydroxamic acid against lung cancer cells. Materials Science and Engineering: C. 2015;51:362-8.
19. Rahman MS, Chowdhury A-N, Rahman M, Islam MM. Drug delivery: Bactericidal effect of manganese oxide-loaded carbon nanotubes enhances drug efficiency. Journal of Biotechnology and Biomedicine. 2022;5(2):137-47.
20. Abdullah JAA, Eddine LS, Abderrhmane B, Alonso-González M, Guerrero A, Romero A. Green synthesis and characterization of iron oxide nanoparticles by pheonix dactylifera leaf extract and evaluation of their antioxidant activity. Sustainable Chemistry and Pharmacy. 2020;17:100280.
21. Claros M, Setka M, Jimenez YP, Vallejos S. AACVD synthesis and characterization of iron and copper oxides modified ZnO structured films. Nanomaterials. 2020;10(3):471.
22. Kwak TW, Kim DH, Jeong Y-I, Kang DH. Antitumor activity of vorinostat-incorporated nanoparticles against human cholangiocarcinoma cells. Journal of nanobiotechnology. 2015;13:1-13.
23. Habeeb SA, Hammadi AH, Abed D, Al-Jibouri LF. Green synthesis of metronidazole or clindamycin-loaded hexagonal zinc oxide nanoparticles from Ziziphus extracts and its antibacterial activity. Pharmacia. 2022;69:855-64.
24. Arunkumar T, Karthikeyan R, Ram Subramani R, Viswanathan K, Anish M. Synthesis and characterisation of multi-walled carbon nanotubes (MWCNTs). International Journal of Ambient Energy. 2020;41(4):452-6.
25. Aslam MM-A, Kuo H-W, Den W, Usman M, Sultan M, Ashraf H. Functionalized carbon nanotubes (CNTs) for water and wastewater treatment: preparation to application. Sustainability. 2021;13(10):5717.
26. Al-Assaly R, Abdulmunem Habeeb S, Hammadi AH, Fadhil Al-Jibouri L, Hameed R, Al-Nafiey A. Antimicrobial performance and instrumental analysis for hexagonal ZnO NPs biosynthesized via Ziziphus leaf extract. Oxford Open Materials Science. 2024;4(1):itae011.
27. Salah LS, Ouslimani N, Bousba D, Huynen I, Danlée Y, Aksas H. Carbon nanotubes (CNTs) from synthesis to functionalized (CNTs) using conventional and new chemical approaches. Journal of Nanomaterials. 2021;2021(1):4972770.
28. Sarode VB, Patil RD, Chaudhari GE. Characterization of functionalized multi-walled carbon nanotubes. Materials Today: Proceedings. 2023.
29. Kani EN, Rafiean AH, Alishah A, Astani SH, Ghaffar SH. The effects of Nano-Fe2O3 on the mechanical, physical and microstructure of cementitious composites. Construction and Building Materials. 2021;266:121137.
30. Rani P, Deshmukh K, Kadlec J, Karthik TK, Pasha SK. Dielectric properties of graphene/nano-Fe2O3 filled poly (vinyl alcohol)/Chitosan blends. Materials Chemistry and Physics. 2023;295:126986.

Cite this article: Abed D, Habeeb SA, Al-Jibouri LF, Hammadi AH, Kbah NZ. Synthesis, Structural Properties and Antibacterial Activity of Vorinostat Loaded on Carbon Nanotubes or Iron Oxide Nanoparticles. Indian J of Pharmaceutical Education and Research. 2026;60(3):1159-68.